Title

Electric Field Polarity Controls Distribution of Viral Bioreceptors within Near-Field Electrospun Biohybrid Microfiber Optical Biosensors

Journal

ACS Applied Bio Materials, 8(3)

ISSN

2576-6422

Authors

Hsieh, Stephen T

Watkins, Jordyn M

Alibay, Zaira

et al.

Publication Date

2025-03-17

DOI

10.1021/acsabm.4c01761

Peer reviewed

ACS Applied Bio Materials 2025 8 (3), 2242-2250

Electric field polarity controls distribution of viral bioreceptors within near-field electrospun biohybrid microfiber optical biosensors

Stephen T. Hsieh[1†], Jordyn M. Watkins[2†], Zaira Alibay[1], Joshua M. Plank[2], Kalie Inouye[3], Nosang V. Myung[4], Elaine D. Haberer[1,2]*

[1]Materials Science and Engineering Program, University of California, Riverside, California 92521, United States.

[2]Department of Electrical and Computer Engineering, University of California, Riverside, California 92521, United States.

[3]Department of Bioengineering, University of California, Riverside, California 92521, United States.

[4]Department of Chemical and Biomolecular Engineering, University of Notre Dame, Notre Dame, Indiana 46556, United States.

†These authors contributed equally.

E-mail address: *haberer@ucr.edu*

ABSTRACT

Microorganisms (e.g. bacteria, fungi, and viruses) add indispensable functionality to a range of electrospun polymer materials and devices. The optimal distribution of bioactive agents on either the interior or exterior of the fiber is application specific. Current microbe surface immobilization strategies and core-confinement techniques continue to pose a number of challenges. Here, we explore a simple strategy, utilizing electrostatic forces, to control the migration and surface concentration of the M13 bacteriophage within near-field electrospun polyvinyl alcohol (PVA) microfibers. Both the surface charge of the electrospun virus and the applied electric field polarity altered microbe placement. When doped with Rhodamine 6G (R6G), the circular microfiber cross-sections formed active whispering gallery mode (WGM) resonators. These relatively high quality (Q) optical cavities enabled us to sensitively probe the virus content of their outer layer, while functioning as label-free optical biosensors with phage-based streptavidin biorecognition elements. Coulomb forces displayed significant control over M13 surface coverage during near-field electrospinning, increasing biosensor response by nearly a factor of four to 1310 nM streptavidin. These findings are an important demonstration of electrostatic forces as a simple, yet adaptable method to enhance biohybrid fiber functionality and performance by tailoring microbe distribution.

KEYWORDS: Near-field electrospinning, Electrical polarity, Whispering gallery mode fiber resonator, Label-free biosensor, M13 bacteriophage

1. INTRODUCTION

Electrospinning is a rapid, low-cost method for manufacturing nano- and microscale fibers. In this simple and scalable process, a strong electric field between spinneret and collector is used to draw fiber from the charged surface of a polymer droplet. Due to its ability to form fibers at room temperature in nonhazardous solvents, electrospinning is particularly attractive for integration of microorganisms (e.g. bacteria, fungi, and viruses). Electrospun biohybrid fibers readily combine the structural properties of polymers with the biofunctionality of microbes. By creating a physical barrier and providing mechanical support, biocompatible polymers can preserve biological activity against harsh environmental and processing conditions[1]. This increases the overall viability and stability of microbial bioactive agents for a wide range of applications including biosensing[2,3], bioscaffolding and regenerative medicine[4–6], bioremediation [7–9], food technology[10] , and green agriculture.[11–13]

Notably, biohybrid fiber functionality and performance depend on the concentration and accessibility of the incorporated microorganisms. Specifically, the local density of microbes within the fiber plays a critical role. Some applications require a high concentration of microorganisms on the fiber surface. As examples, biorecognition elements on an actuator surface enable precise and selective analyte concentration measurement[3] and surface-functionalized bioscaffolds promote cellular growth, proliferation, and differentiation.[5,14,15] Other applications are better served by positioning microbes in the interior of the fiber. For instance, encapsulated bioactive agents subvert immune response for sustained viral gene transfer[6] and sub-surface bioremediators enhance viability for extended pollutant degradation.[9] Yet, current microbe surface immobilization strategies and core-confinement techniques pose challenges. Surface adsorption and covalent surface attachment represent a trade-off between potential

operational instability due to uncontrolled desorption and partial microbe inactivation[16,17] whereas coaxial and emulsion electrospinning require careful material selection to manipulate core-shell interfacial tension.[16] Moreover, both post-processing surface functionalization techniques and co-electrospinning methods add a degree of complexity to fiber preparation.

An alternative, and rather unexplored approach, is to exploit electrospinning polarity to control local microbe density. Most biological materials, including microorganisms, carry a net charge. The magnitude and sign of their surface charge is dependent on their isoelectric point and the solution pH. Surface charge can be used in conjunction with electric field polarity to preferentially attract or repel charged biological entities within the polymer solution to or from the fiber surface. This approach has been demonstrated for a range of biomolecules and bioactive components including proteins[18], natural carbohydrates or polysaccharides[19–21], and therapeutics[22] , but has been largely overlooked for control of larger biologics such as micro-organisms.

In this work, the effects of pH and polarity on the migration and surface concentration of M13 bacteriophage within blended near-field electrospun (NFES) polyvinyl alcohol (PVA)/phage microfibers were examined. There is growing interest in electrospinning this highly adaptable filamentous virus for stabilization and storage applications[23], sensors[3], tissue-engineering scaffolds[4,24,25], and energy harvesting[26]. The nearly one micron long and 6.5 nm diameter M13 phage can be functionalized with a variety of moieties utilizing either genetic or chemical means. Moreover, it tolerates a large pH range[27], thus enabling significant surface charge manipulation. As shown in Figure 1, a streptavidin-binding M13 variant was mixed and electrospun with PVA, a neutral and biocompatible polymer. By spinning above and below the isoelectric point of the variant with both positive and negative electric field polarities, the contribution of electrostatic

Coulomb forces in controlling the phage distribution within the fiber was assessed. Fiber morphology and size, as well as the internal dispersion of bacteriophage were characterized with optical and confocal fluorescence microscopy. M13 surface density was evaluated using scanning electron microscopy to complement streptavidin-conjugated Au nanoparticle binding experiments. Coulomb forces associated with the net surface charge of the M13 variant and electrospinning polarity influenced its migration, considerably modifying the M13 concentration on the fiber exterior. Subsequently, the M13/PVA biohybrid microfibers were doped with Rhodamine 6G (R6G) to form optically active whispering gallery mode (WGM) resonators. Using the high quality (Q) modes supported by their circular cross-sections, the virus content of the outer layer was further investigated. Finally, label-free optical biosensors with phage-based streptavidin biorecognition elements were fabricated. In recent years, the M13 bacteriophage has gained interest as an alternative affinity-based bioreceptor due to its extraordinary multivalency and robustness, in addition to the availability of comparatively low cost manufacturing methods. Using electrostatic Coulomb forces, M13 bioreceptor surface coverage was enhanced from approximately 3.42% to 12.76% in 1310 nM streptavidin solution, leading to a remarkable 3.7x increase in biosensor optical response. These studies are an important demonstration of Coulomb interactions as a simple, yet highly versatile tool to improve biohybrid fiber functionality and performance by tailoring microbe distribution.

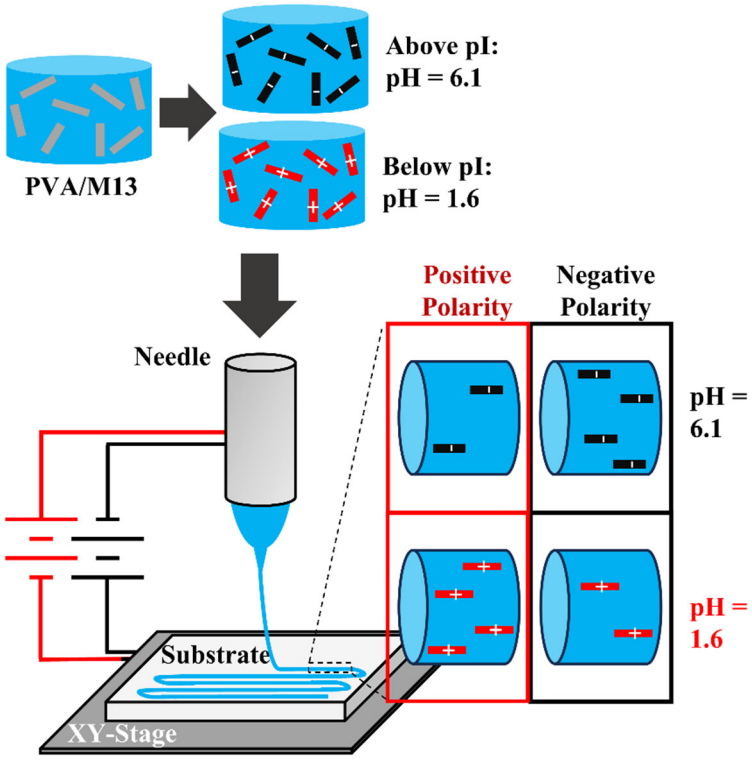

Figure 1. Schematic of biohybrid electrospinning approach utilizing filamentous M13 bacteriophage with different surface charges and electrospinning polarity to control virus distribution.

2. MATERIALS AND METHODS

2.1 Modification and amplification of M13 filamentous phage.

Following a previously reported procedure, the M13 bacteriophage, a rod-shaped virus 880 nm in length and 6.5 nm in diameter, was genetically altered to bind to streptavidin.[28–30] The pVIII major coat protein, located along the length of the virus in high copy number (>2700), was modified to include a streptavidin-binding peptide fusion (VPEGAFSS[30]) near the N-terminus. The streptavidin-binding phage variant was amplified and purified as previously described.[29] The final phage solution was suspended in 0.1X phosphate buffer saline (PBS, 13.7 mM NaCl, 0.27 mM KCl, 1 mM Na_2HPO_4, 0.18 mM KH_2PO_4) at 1 mg/ml and stored at 4°C until use.

2.2 Preparation and characterization of PVA/M13 electrospinning solutions.

Electrospinning solutions were prepared by mixing polyvinyl alcohol (PVA, 13,000-23,000 g/mol, 98% hydrolyzed, Sigma Aldrich) with deionized water at 27% w/w. Solutions were stirred for 2 h at 80℃ until the PVA was fully dissolved, then allowed to cool for 30 min. PVA/M13 solutions were formed by adding streptavidin-binding bacteriophage in 0.1X PBS to reach the desired 25% w/w PVA with 0.1 mg/ml virus loading. Control solutions of 25% w/w PVA were also made by adding 0.1X PBS alone. Solutions were subsequently stirred at room temperature for another 30 min to ensure homogeneity.

The surface charge of the streptavidin-binding phage was measured in PBS with a Zetasizer (NanoZS90, Malvern Instruments) using 5 M HCl and 1 M NaOH to adjust pH. A minimum of 8 measurements were averaged at each condition. Following a report by Passaretti[31], a fifth order polynomial was used to fit the data. UV-Vis spectroscopy (Evolution 60, ThermoFisher) was used

to evaluate the optical transmission of PVA/M13 and PVA solutions above and below the isoelectric point of the streptavidin-binding phage. Spectra were baselined using the absorption spectrum of PBS. A fluorescent dye, Rhodamine 6G (R6G, Sigma Aldrich), was incorporated into polymer solutions at a concentration of 0.0117 mg/ml to serve as an optical emitter for WGM resonance applications.

2.3 Near-field electrospinning (NFES) and glutaraldehyde crosslinking of PVA/M13 fibers.

Prior to electrospinning, glass substrates (14 x 14 x 1 mm) were prepared by scribing parallel trenches into the surface.[32] The substrates were sequentially immersed and sonicated (FS20 Ultrasonic Cleaner, Fisher Scientific) in acetone, isopropanol, and deionized water for 30 min to clean the surface. A programmable X-Y stage (A-LSQ300D, Zaber) held and translated the substrates during spinning. A point-plate near-field electrospinning (NFES) configuration with a separation of 1.25 mm between the needle tip and substrate was used to fabricate micron-scale PVA/M13 and PVA fibers. Polymer solution was loaded into a syringe with an attached stainless steel 27-gauge blunt-tip needle (Fisnar). Using a syringe pump (NE 300 US, New Era Syringe Pump), electrospinning solution flowed at a rate of 10 μL/h.

To achieve blended electrospun fibers from the polymer solutions, two separate high voltage power supplies (P03.5HA8.5/N03.5HA8.5, Acopian Technical Company) were used: one positive and one negative. The electrospinning polarity was changed by designating the power supply connected to the spinneret needle. For positive polarity NFES, the positive power supply was attached to the needle and the negative power supply was attached to the collector stage. The leads were switched for negative polarity NFES. In both cases, |1.9 kV| was applied to the needle and |0.1 kV| was applied to the collector to maintain a 2.0 kV voltage drop. The X-Y stage was

programmed to move at a rate of 0.5 mm/s in a parallel-line pattern, producing fibers approximately 10 mm long and 200 μm apart. Fibers were written perpendicular to the trenches scribed into the glass substrate, allowing them to be suspended and optically isolated for whispering gallery mode measurements.

For aqueous experiments, the PVA/M13 and PVA fibers were crosslinked using glutaraldehyde (GA, Fisher Scientific) with hydrogen chloride (HCl) as a catalyst.[32] Fibers were placed in a closed chamber and exposed to vapor from a 50% w/w GA solution and 1 M HCl for 24 h followed by a second vapor treatment step with 50% w/w GA solution and 5 M HCl for 24 h. Finally, the fibers were soaked in 50% w/w GA solution for 24 h, rinsed with deionized water to remove excess GA, and dried in a vacuum desiccator.[32]

2.4 Characterization of electrospun PVA/M13 fibers.

The size of the electrospun fibers was measured with an optical microscope (LabRam LabSpec6, Horiba Scientific). Edges of the fibers were brought into focus using 50x long working distance objective, and then dimensions were acquired with a built-in digital measuring tool. Confocal fluorescence microscopy (Leica SP5) was used to characterize the distribution and size of the filamentous virus within the fibers. For these experiments only, the streptavidin-binding M13 bacteriophage were tagged with a fluorescent dye using an NHS-amine reactive process (DyLight™ 550 NHS Ester, Thermo Scientific) and electrospun. The biohybrid fibers were imaged under 543 nm laser excitation. Emitted dye fluorescence indicated the location of the M13 virus. Images were analyzed using image processing software (ImageJ). For each electrospinning condition, the length and nearest neighbor distance (NND) of the M13 aggregates were measured on three different samples with a minimum N value of 100.

The amount of M13 variant on the fiber surface was evaluated using a lower concentration of streptavidin-conjugated Au nanoparticles (50 nm dia., Cytodiagnostics; 0.583 nM). To reduce non-specific binding, the fibers were immersed in bovine serum albumin (BSA, 1 mg/ml) solution as a blocking agent for 30 min, then rinsed ten times with deionized water and dried in vacuum. Afterwards, the streptavidin-coated Au nanoparticles were incubated with the crosslinked PVA/M13 fibers for 3 h. The fibers were again rinsed ten times with water, dried 24 h, and imaged with scanning electron microscopy (SEM). Areal densities of bound Au nanoparticles were determined by counting the number of particles (ImageJ) and dividing by the corresponding fiber surface area. For each electrospinning condition, at least five fibers were measured across three samples ($N > 15$).

2.5 Whispering gallery modes (WGMs) as optical probes and label-free streptavidin biosensors.

A far-field laser confocal system (LabRam, Horiba Scientific) was used to excite whispering gallery modes (WGMs) in R6G PVA and PVA/M13 fibers, similar to a previous report.[32] A 532 nm continuous wave laser light (Ventus, Laser Quantum) was focused using a 50x objective (NA = 0.75), resulting in a spot size of approximately 3 μm and an incident laser power of 6 μW to excite R6G inside the fibers. The emitted fluorescence was collected using the same objective and the light was directed into a spectrometer with an 1800 lines/mm diffraction grating and a charge-coupled device detector. The resulting spectrum had a spectral resolution of 0.014 nm.

To calculate resonator refractive index and Q-factor, a random selection of uncrosslinked PVA and PVA/M13 resonators roughly representing the fiber diameter distribution were excited with the far-field laser confocal system while suspended in air. The resulting WGM spectra were

analyzed by subtracting the broad R6G fluorescence emission. Resonant modes were fitted with Lorentzian functions to determine the peak position and width. Cavity Q-factors were calculated using

$$Q = \frac{\lambda_{Resonance}}{\lambda_{FWHM}} \quad (1)$$

where $\lambda_{Resonance}$ is the position and λ_{FWHM} is the full-width half maximum of the resonant peak. The Q factor was calculated for a minimum of 37 unique resonators at each fiber fabrication condition. Mode numbers were assigned and resonator refractive indices were extracted using a Mie-theory approximation[33,34]:

$$\lambda \cong \pi n_{res} D \left[\nu + \frac{\alpha_s \nu^{\frac{1}{3}}}{2^{\frac{1}{3}}} - \frac{P}{(m^2-1)^{\frac{1}{2}}} + \frac{3}{10} \frac{\alpha_s{}^2}{2^{\frac{2}{3}} \nu^{\frac{1}{3}}} - \frac{P\left(m^2 - \frac{2P^2}{3}\right)}{(m^2-1)^{\frac{3}{2}}} \frac{\alpha_s}{2^{\frac{1}{3}} \nu^{\frac{2}{3}}} \right]^{-1} \quad (2)$$

where D is the optically measured fiber diameter, ν is the angular mode number (l) plus 0.5, α_s are the roots of the Airy function, and n_{res} is the refractive index of the resonator. The term m is the ratio of the refractive index of the resonator to the refractive index of the surrounding medium (n_{res}/n_{surr}) while P is 1/m for transverse magnetic (TM) modes and m for transverse electric (TE) modes. TM modes are defined with electric field vector perpendicular to the resonator surface while TE modes are modes with the electric field vector parallel to fiber axis. The best computed solutions were evaluated using the least mean residual squared. The n_{res} was approximated for a minimum of 6 resonators at each fiber fabrication condition with diameters ranging from 4 to 14 μm.

In preparation for WGM biosensing experiments and to reduce non-specific binding, biohybrid crosslinked devices were first immersed in bovine serum albumin (BSA, 1 mg/ml) solution as a blocking agent for 30 min, then rinsed ten times with deionized water and dried in vacuum. The

devices were submersed in a 1X PBS (137 nM NaCl, 2.7 mM KCl, 10 mM Na_2HO_4, 1.8 mM KH_2PO_4) bath at least 1 h prior to WGM excitation to allow stabilization. WGM spectra were recorded repeatedly at 3 min intervals for a minimum of 1 h in the PBS bath. Subsequently, the devices were exposed to streptavidin (1310 nM). The shift in WGM resonance was recorded over a period of at least 1 h. The spectral shift was calculated from peak positions 15 min before and after the addition of streptavidin for at least three samples at each condition. Presuming a single layer of randomly bound streptavidin proteins to the resonator, the surface density of bound streptavidin to the biohybrid PVA/M13 fiber biosensors was estimated through the observed spectral shift by utilizing the equation

$$\frac{\Delta\lambda}{\lambda} = \frac{\alpha_{ex}\sigma_p}{\varepsilon_0(n_{res}{}^2 - n_{surr}{}^2)R} \quad (3)$$

where α_{ex} is the excess polarizability of streptavidin ($4\pi\varepsilon_0 \bullet 3.85\times10^{-21}$) cm^3 [35], R is the radius of the resonator, n_{res} is the index of refraction of the PVA fiber (1.464)[32], and n_{surr} is the index of refraction of the surrounding PBS (1.3338), and σ_p is the surface density of the bound streptavidin. Assuming streptavidin is a 5 nm sphere and a square close-packed monolayer, the maximal surface density of streptavidin is 4×10^{12} streptavidin/cm^2. [36]

3. RESULTS AND DISCUSSION

3.1 M13 surface charge modification.

Zeta potential was measured as a function of pH to determine the surface charge and isoelectric point (pI) of the streptavidin-binding M13 variant used in these studies. The net charge of this filamentous virus depends on the number of exposed, ionizable amino acids on the capsid surface, as well as the degree of ionization of those residues. The M13 viral capsid is composed

of five structural proteins. Its surface charge is dominated by the pVIII major coat protein that is found along the length of the nearly one micrometer filament in high copy number (>2700). Notably, the pVIII coat of the streptavidin-binding phage variant has one less ionizable amino acid than that of the wild type or unmodified phage.[30] As shown in Figure 2, the isoelectric point of the streptavidin-binding phage was approximately 5.3, slightly higher than the wild type.[31] Two electrospinning solutions were prepared in order to investigate the influence of electrostatic forces on PVA/M13 near-field electrospun: one in which the streptavidin-binding M13 surface charge was positive (pH 1.6) and one in which it was negative (pH 6.1).

As shown in Figure 2, with the addition of a low concentration (0.1 mg/ml) of M13 variant, the optical transmission at pH 6.1 was reduced by 23% at 600 nm, yet it remained unchanged at pH 1.6. These observations were stable with time (Figure S1). The reduced transmission was ascribed to light scattering by M13 aggregates. Non-adsorbing polymers such as PVA tend to induce phase separation of high aspect ratio viruses through osmotic pressure[37]. Nonetheless, the pH 1.6 PVA/M13 solution demonstrates that repulsive electrostatic forces can be engineered to, at least partially, counterbalance these attractive forces. This tunability is important for biohybrid fiber applications in which homogeneous microorganism dispersion is critical. In particular, for the whispering gallery mode resonators studied here, losses associated with M13 aggregates can affect optical cavity performance.

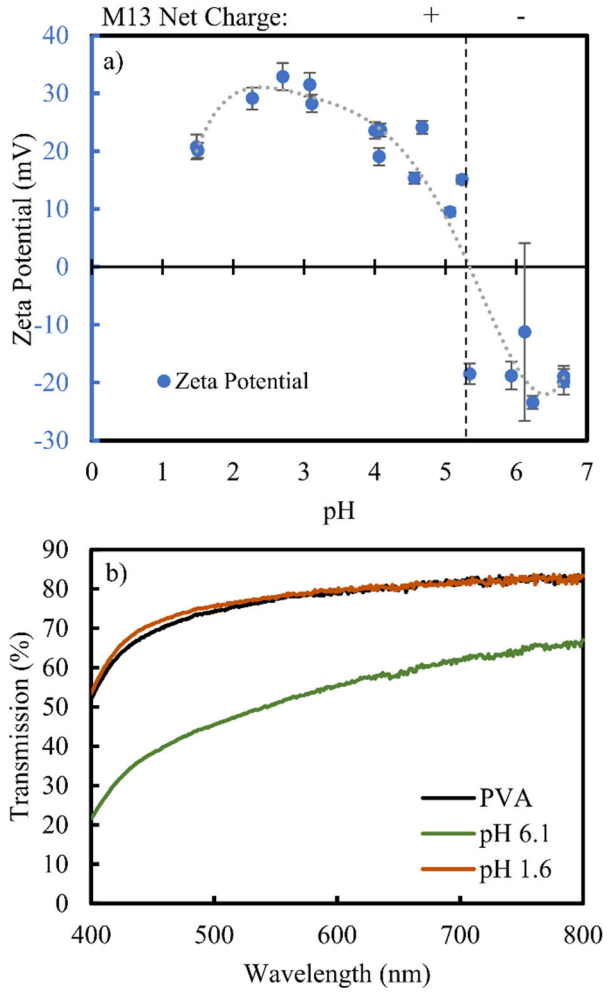

Figure 2. a) Zeta potential measurements of the streptavidin-binding phage variant as a function of pH. For these experiments, the phage were dispersed in aqueous solution. A fifth order polynomial was used to fit the data and approximate the isoelectric point of the virus. b) Optical transmission spectra of PVA/M13 electrospinning solutions above and below the isoelectric point of the streptavidin-binding variant. M13 bacteriophage does not absorb in this spectral range. A transmission spectrum of a PVA electrospinning solution without phage is shown for comparison.

3.2 Effects of pH and electrospinning polarity on PVA/M13 microfibers.

Both pH 1.6 and pH 6.1 PVA/M13 solutions were blend electrospun with either a positive or a negative applied voltage on the spinneret needle. As depicted in Figure 1, this allowed for exploration of electrostatic Coulomb forces using all combinations of virus surface charge and electrospinning field polarity. As shown in Figure S2, continuous PVA microfibers with incorporated M13 bacteriophage were readily electrospun; no bead formation was observed. The size distributions of fibers fabricated with each condition and measured with optical microscopy are shown in Figure 3. Notably, fibers electrospun at pH 6.1 averaged two microns larger than those electrospun at pH 1.6. On the contrary, the electric field polarity had comparatively little effect on average PVA/M13 electrospun microfiber diameter.

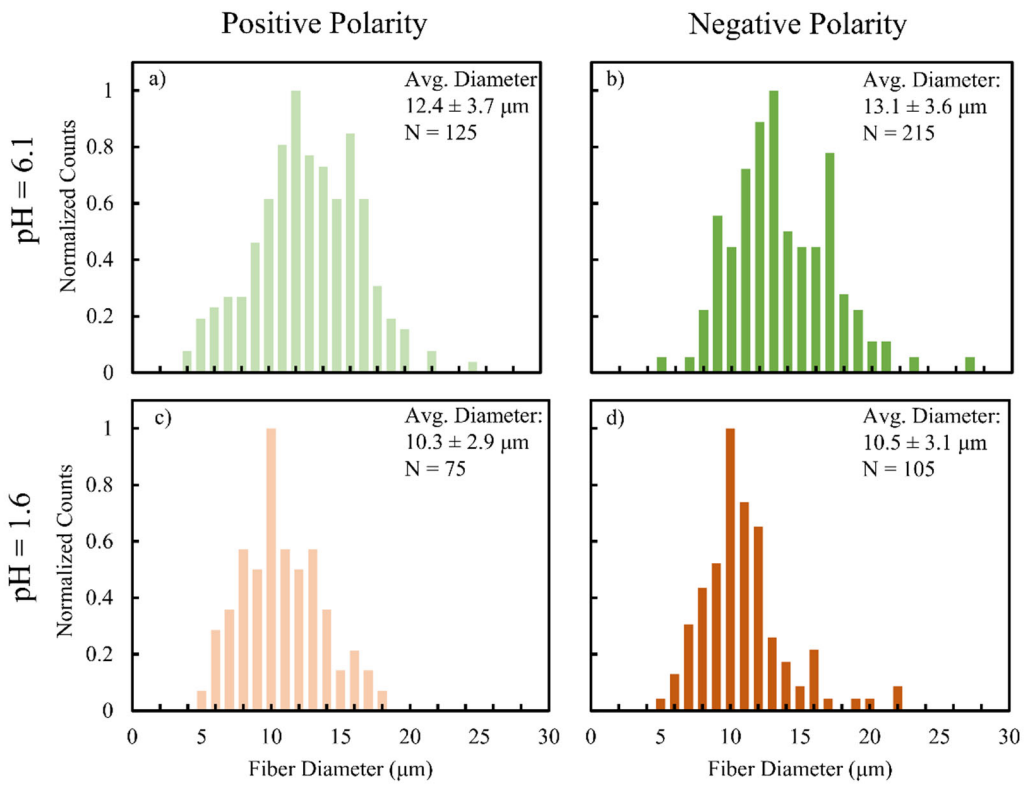

Figure 3. Histograms of electrospun PVA/M13 fiber size, as measured with optical microscopy. Solutions were electrospun with (a, b) pH 6.1 and (c, d) pH 1.6. The polarity of the applied electric field was (a, c) positive and (b, d) negative.

Confocal fluorescence microscopy was used to evaluate the dispersion of the streptavidin-binding variant within the PVA/M13 microfibers. For these experiments, the M13 variant was fluorescently tagged prior to mixing with PVA solution. Despite the relatively high transmission of the pH 1.6 solution prior to spinning, bright fluorescent areas longer than the length of an individual virus filament and consistent with the formation of large oblong bundles of phage were observed within the microfibers under all conditions. Representative bright field and confocal fluorescence microscopy images of fibers electrospun at pH 6.1 and pH 1.6 with positive polarity are found in Figure 4, along with average M13 bundle length and nearest neighbor distance for each electrospinning condition. Histograms of phage bundle length and spacing are also included in Figures S3 and S4. Aggregates found in fibers spun at pH 6.1 were more polydisperse, longer and further apart than in fibers spun at pH 1.6. Increased scattering due to the larger aggregates within the distribution likely caused the disparity in solution optical properties. Analogous images of biohybrid fibers electrospun with negative polarity have been included in Figure S5, for comparison. Similar pH-dependent trends were found, but no significant differences were observed for electrospinning polarity. To demonstrate uniformity of aggregate length and spacing across samples, additional confocal images are included in Figure S6 for each electrospinning condition.

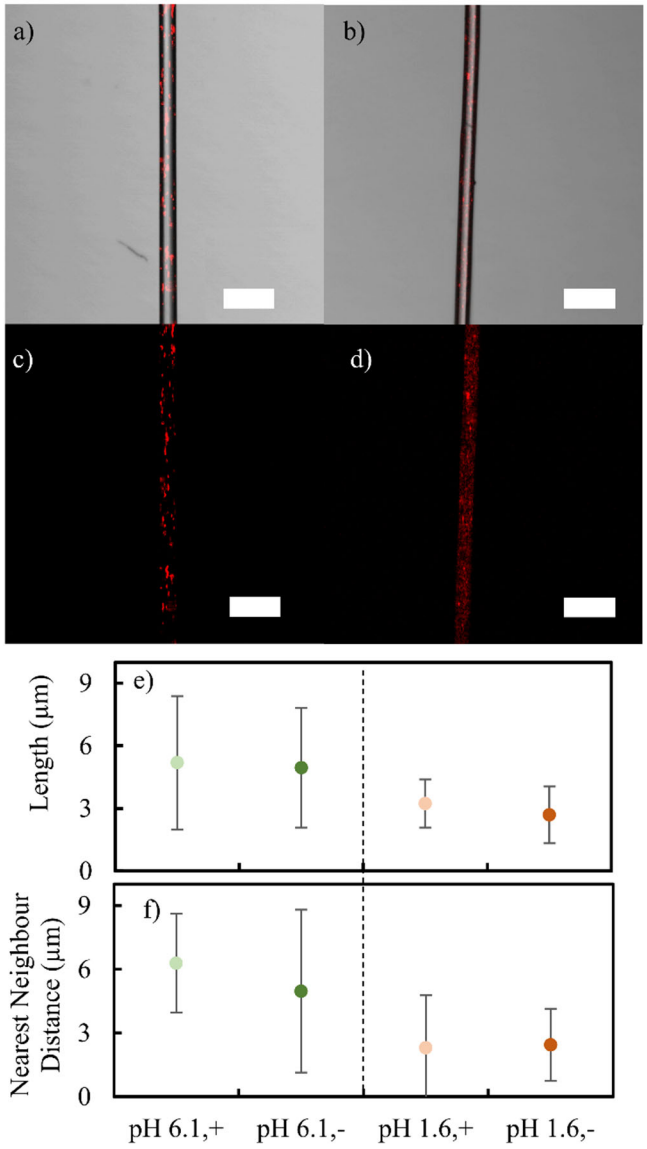

Figure 4. Confocal optical microscope images using dye-tagged phage to visualize the M13 streptavidin-binding variant within fibers electrospun with positive polarity. Representative bright field images overlayed with fluorescence emission and isolated fluorescence emission for fibers spun with positive electric field polarity at (a, c) pH 6.1 and (b, d) pH 1.6. Scale bar: 50 µm. Measured (e) length and (f) spacing of phage agglomerates for four combinations of solution pH and applied electric field polarity. Confocal fluorescence contrast was increased for pH 1.6 images. (N > 100)

The affinity of the genetically modified M13 variant for streptavidin was used to assess the effects of net charge and electrospinning polarity on phage surface concentration. Following incubation with a low concentration of 50 nm streptavidin nanoparticle conjugates, fibers were imaged with electron microscopy to quantify the attached particles. Figure 5 depicts a representative fiber with streptavidin conjugated Au nanoparticles bound to it. In addition, to illustrate uniformity, a low magnification and several high magnification electron microscopy images of the PVA/M13 fibers are included in Figures S7 and S8, respectively. Average particle surface densities were evaluated for PVA/M13 and PVA control fibers and plotted in Figure 5.

Biohybrid fibers were initially electrospun at pH 1.6 with either positive or negative polarity applied to the spinneret. Below the isoelectric point of the streptavidin-binding phage, the net charge of the M13 variant was positive. With a positive voltage applied, the particle surface density was 3.0x that of fibers spun with a negative voltage. During the blend electrospinning process, attractive electrostatic forces cause negatively charged species within the solution to migrate toward the positively polarized needle. These species become immobilized on the needle, leaving a surplus of positively charged species, such as the M13, within the solution.[38,39] For this reason, fibers spun with positive polarity were enriched with streptavidin-binding phage while fibers spun with negative polarity were depleted. For a solution spun at pH 6.1, no significant difference was observed in particle surface density. This result was attributed to the comparatively slower migration of the large phage agglomerates at pH 6.1 in response to electrostatic forces.

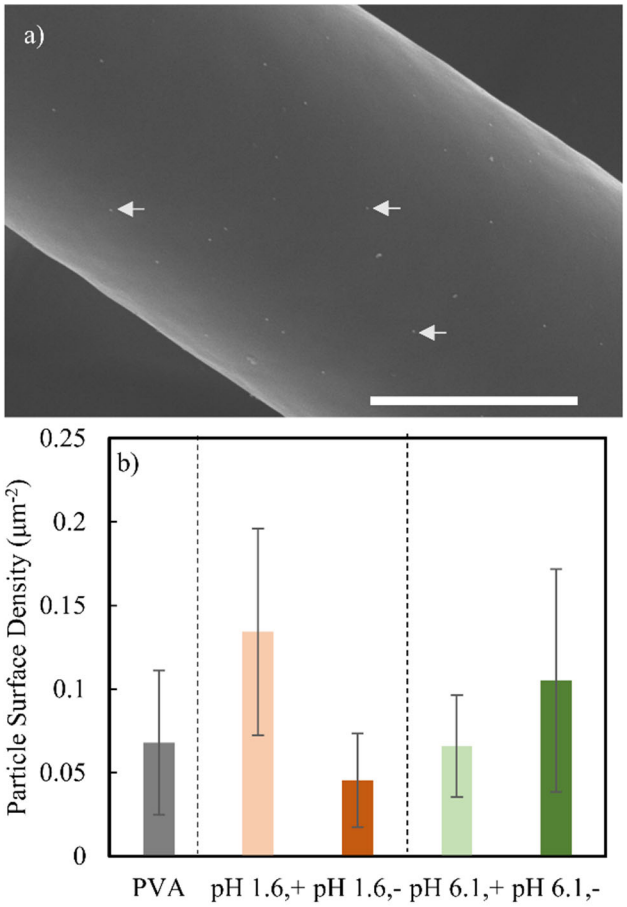

Figure 5. a) SEM image of 50 nm diameter nanoparticle conjugates on crosslinked PVA/M13 fiber surface. White arrows indicate the positions of a few representative nanoparticles. Scale bar: 5 μm. b) Surface density of nanoparticle conjugates bound to electrospun fibers for all four combinations of solution pH and applied electric field polarity. ($N > 15$)

3.3 Whispering gallery mode (WGM) resonators as optical probes of electrospun M13 distribution.

PVA/M13 microfibers electrospun at pH 1.6 were selected for additional investigation as WGM resonators. Lower pH solutions had greater optical transmission. Furthermore, fibers electrospun from these solutions had smaller phage aggregates and potentially larger M13 surface densities, making them more suitable for optical resonators and label-free biosensors. As shown in Figure 6, WGM resonators are simple, radially symmetric high quality (Q) optical cavities (e.g. cylindrical fibers, spheres, rings, etc.)[40–43] that support considerable light recirculation due to total internal reflection. Resonances appear as sharp peaks on a broad fluorescence background. First order WGMs, such as those in these experiments, are typically confined within a narrow radial distance x from the cavity periphery such that $0.9r < x < r$, where r is the radius of the fiber.[44] Their resonance is affected by tiny changes in refractive index, path length, and scattering centers, making them highly sensitive measurement tools near the fiber perimeter.[45,46] The WGMs supported within the circular cross-sections of the electrospun microfibers served as a convenient means with which to probe the outer layer of the biohybrid materials. These experiments were completed to learn more about the electrostatically controlled M13 distribution, as well as its effect on the optical cavity performance.

WGMs were excited in dye-doped PVA/M13 microfibers electrospun at pH 1.6 with positive and negative electric field polarities. Dye-doped PVA fibers spun without the addition of the M13 variant also supported WGMs. For modal analysis, each resonance peak was fit with a Lorentzian function. Using a Mie-theory derived asymptotic approximation, theoretical spectra were computed and best-fit values were extracted for the fiber refractive indices for a minimum of 6 samples at each condition..[33,34] The PVA fibers had a refractive index of 1.4583 ± 0.0091.

The inclusion of streptavidin-binding phage raised refractive indices for fibers spun with positive and negative polarity to 1.5047 ± 0.0222 and 1.4868 ± 0.0320, respectively. The increase was attributed to the presence of the M13 filamentous virus, a higher refractive index biomaterial (n ~1.57)[47,48], within the modal volume. Fibers spun with positive polarity had a larger refractive index due to the higher concentration of streptavidin-binding phage within the outer layer of the fiber. Cavity Q values were also calculated and are plotted as a function of diameter in Figure S9. This figure of merit is inversely proportional to optical loss (e.g. radiative, scattering, and absorption losses) and can provide additional information regarding near-surface microbe distribution. For smaller diameter fibers, radiative or geometry dependent losses tended to dominate. Little difference was observed with the addition of the M13 variant. However, for larger diameter fibers, a different trend was found. Cavity Q was somewhat reduced by the incorporation of filamentous phage, despite the larger refractive indices of these fibers. This decrease was ascribed to scattering losses caused by the presence of phage aggregates. Importantly, Q values were slightly lower for fibers spun with positive polarity than negative. The larger number of phage aggregates near the fiber surface intensified scattering losses. While streptavidin conjugate studies examined only the fiber exterior, these experiments expanded the investigation to the subsurface modal volume. These observations are consistent with the size of the aggregates observed with confocal and have implications for other biohybrid fiber applications.

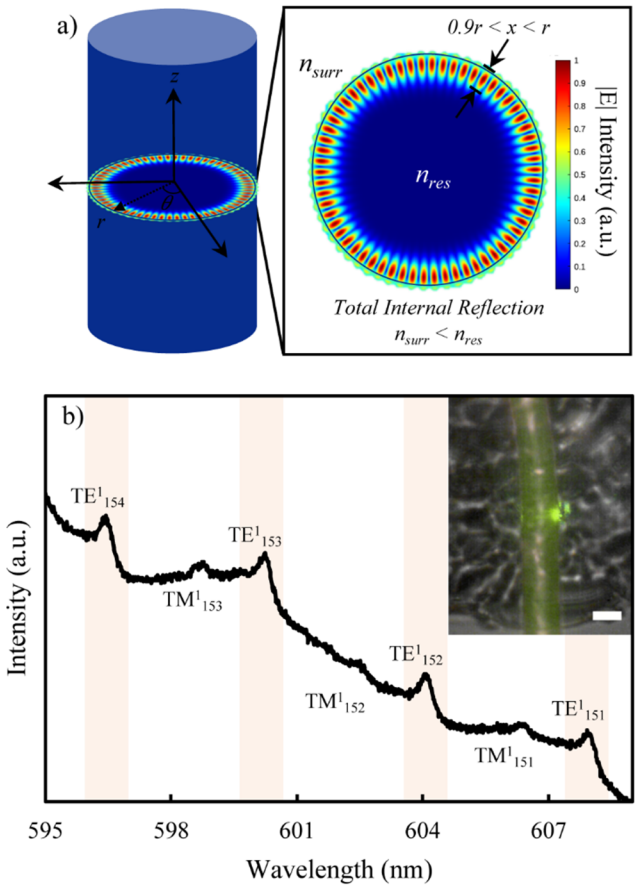

Figure 6. a) Graphical representation of a cylindrical WGM resonator supporting light recirculation within the cross-section due to total internal reflection. b) Representative fluorescence spectrum of a crosslinked BSA blocked 19.41 µm diameter PVA/M13 pH 1.6 fiber electrospun with positive polarity, submerged in PBS. The spectrum was taken with a 50x long working distance objective under 532 nm CW illumination. Inset: Optical image of 18.48 µm diameter PVA/M13 pH 1.6 positive polarity fiber in PBS. Scale bar: 15 µm.

3.4 Control of M13 bioreceptor surface concentration in electrospun label-free WGM biosensors.

Label-free optical biosensing of streptavidin was performed using PVA/M13 microfibers electrospun at pH 1.6 with both positive and negative spinneret polarity. The M13 streptavidin-binding variant served as a biorecognition element, conferring specificity for the analyte to the WGM resonator. A representative spectrum and an optical image of a fiber biosensor immersed in PBS are shown in Figure 6. Fiber resonators with diameters between 16 and 20 μm, and Q values between 2000 and 5000 were selected for sensing experiments. Prior to the addition of streptavidin, the resonance of the fiber was recorded for a minimum of 1 h at 3 min intervals. Streptavidin was added to obtain a 1310 nM solution. The optical responses of the sensors are found in Figure 7. Regardless of polarity, the increased streptavidin concentration caused a rapid increase in resonance wavelength. Streptavidin has a higher polarizability than PBS buffer. As streptavidin displaces the buffer by binding to phage-based bioreceptors on the resonator surface, interactions with the evanescent field cause the WGMs to red shift. Devices electrospun with positive and negative polarity exhibited average red shifts of 0.055 ± 0.031 nm and 0.015 ± 0.033 nm, respectively. In WGM evanescent sensing, only bioreceptors on the cavity surface can participate in analyte binding and detection. The nearly 3.7x larger response measured for the resonators spun with positive polarity is consistent with the higher M13 surface concentration observed in nanoparticle conjugate binding, refractive index, and Q value studies. Using the mode shift of the WGM resonator, the surface density of streptavidin bound to the exterior of the biosensors was calculated.[35] Average surface densities of 1.74×10^{11} streptavidin/cm^2 and 6.05×10^{11} streptavidin/cm^2 were determined for devices spun with negative and positive polarity, respectively. Assuming the streptavidin surface coverage approximately corresponds to that of

the streptavidin-binding phage, by simply switching the spinneret polarity from negative to positive, bioreceptor coverage increased from 3.42% to 12.76%. With extended sensing time, the mode gradually drifted to shorter wavelengths. While the exact source of this blue shift requires further investigation, it is likely due to a combination of fluorescent molecule photobleaching and polymer matrix heating associated with continuous wave laser excitation.

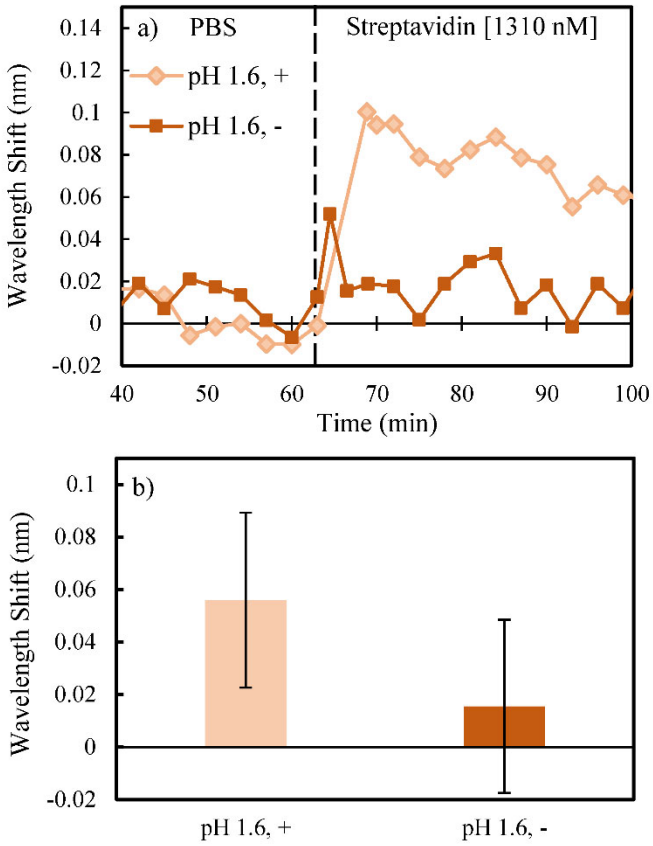

Figure 7. a) Representative resonance peak wavelength shift over time for BSA blocked PVA/M13 pH 1.6 negative and positive polarity devices submerged in PBS and upon exposure to streptavidin solution. b) The WGM resonant shift in response to streptavidin addition averaged from three devices electrospun with a positive polarity and four devices electrospun with a negative polarity.

4. CONCLUSION

In conclusion, we have investigated the role of electrostatic forces on the distribution of a M13 streptavidin-binding variant within PVA near-field electrospun microfibers. For this purpose, the effects of pH and field polarity were explored. Confocal fluorescence microscopy revealed that, while the pH of the electrospinning solution strongly influenced fiber size and phage-phage interactions, polarity did not. In addition, affinity-based nanoparticle conjugate surface binding provided evidence that Coulomb interactions were able to manipulate phage migration and generate biohybrid fibers with surfaces either enriched or depleted of M13.These findings represent an opportunity to use electrospinning polarity to maintain microbe surface presentation, while tailoring microfiber dimensions and microorganism dispersion independently through pH or other solution parameters.[37] The circular cross-sections of fluorescent dye-doped PVA/M13 microfibers were employed as label-free WGM optical resonators to further probe microbe position and detect streptavidin as a model bioanalyte. Modal analysis, which extended the investigation to the near surface microbe content, supported nanoparticle binding affinity findings. The significant polarity-driven increase in phage bioreceptor surface density resulted in a 3.7x enhancement in biosensor response. These studies validate electrostatic forces as a simple, yet highly effective means to control microorganism surface concentration within biohybrid near-field electrospun fibers, drastically improving performance. Moreover, the combination of this strategy and WGM resonator fabrication demonstrates the potential of integrated electrospun biohybrid sensors for a range of applications from detection of metabolites near bioscaffolds to pollutant degradation caused by encapsulated bioremediators.

ASSOCIATED CONTENT

Supporting Information. Time-dependent transmission spectra of electrospinning solutions; optical microscopy images of the electrospun fibers; histograms of M13 fiber bundle length and nearest neighbor distances; both low and high magnification confocal fluorescence microscopy images of biohybrid electrospun fibers revealing aggregate size and spacing; both low and high magnification electron microscopy images of nanoparticle conjugate binding; Q values as a function of fiber diameter for PVA and PVA/M13 fibers. Supporting information for this article can be found online.

AUTHOR INFORMATION

Corresponding Author

Elaine D. Haberer – Department of Electrical and Computer Engineering, University of California, Riverside, California 92521, United States; Materials Science and Engineering Program, University of California, Riverside, California 92521, United States; http://orcid.org/0000-0002-3676-9079; Email: haberer@ucr.edu

ACKNOWLEDGMENT

This material is based upon work supported by the National Science Foundation under Grant No. ECCS-1406795. The UCR CoR Grant Program provided additional support. S.T.H. is grateful for support from the U. S. Department of Education via the Graduate Assistance in Areas of National Need (GAANN) program under award number P200A210031. In addition, this study utilized the Analytical Chemistry Instrumentation Facility, the Institute for Integrative Genome Biology, and the Central Facility for Advanced Microscopy and Microanalysis at University of California, Riverside.

REFERENCES

(1) Balusamy, B.; Sarioglu, O. F.; Senthamizhan, A.; Uyar, T. Rational Design and Development of Electrospun Nanofibrous Biohybrid Composites. *ACS Appl. Bio Mater.* **2019**, *2* (8), 3128–3143. https://doi.org/10.1021/acsabm.9b00308.

(2) Gordegir, M.; Oz, S.; Yezer, I.; Buhur, M.; Unal, B.; Demirkol, D. O. Cells-on-Nanofibers: Effect of Polyethyleneimine on Hydrophobicity of Poly-Ɛ-Caprolacton Electrospun Nanofibers and Immobilization of Bacteria. *Enzyme Microb. Technol.* **2019**, *126* (February), 24–31. https://doi.org/10.1016/j.enzmictec.2019.03.002.

(3) Hsieh, S. T.; Cheeney, J. E.; Ding, X.; Myung, N. V.; Haberer, E. D. Near-Field Electrospinning of Polymer/Phage Whispering Gallery Mode Microfiber Resonators for Label-Free Biosensing. *Sensors Actuators B Chem.* **2022**, *367* (May), 132062. https://doi.org/10.1016/j.snb.2022.132062.

(4) Lee, J. Y.; Chung, J.; Chung, W. J.; Kim, G. Fabrication and in Vitro Biocompatibilities of Fibrous Biocomposites Consisting of PCL and M13 Bacteriophage-Conjugated Alginate for Bone Tissue Engineering. *J. Mater. Chem. B* **2016**, *4* (4), 656–665. https://doi.org/10.1039/c5tb01748c.

(5) Shin, Y. C.; Kim, C.; Song, S.-J.; Jun, S.; Kim, C.-S.; Hong, S. W.; Hyon, S.-H.; Han, D.-W.; Oh, J.-W. Ternary Aligned Nanofibers of RGD Peptide-Displaying M13 Bacteriophage/PLGA/Graphene Oxide for Facilitated Myogenesis. *Nanotheranostics* **2018**, *2* (2), 144–156. https://doi.org/10.7150/ntno.22433.

(6) Liao, I.-C.; Chen, S.; Liu, J. B.; Leong, K. W. Sustained Viral Gene Delivery through Core-

Shell Fibers. *J. Control. Release* **2009**, *139* (1), 48–55. https://doi.org/10.1016/j.jconrel.2009.06.007.

(7) Sarioglu, O. F.; Keskin, N. O. S.; Celebioglu, A.; Tekinay, T.; Uyar, T. Bacteria Encapsulated Electrospun Nanofibrous Webs for Remediation of Methylene Blue Dye in Water. *Colloids Surfaces B Biointerfaces* **2017**, *152*, 245–251. https://doi.org/10.1016/j.colsurfb.2017.01.034.

(8) Desitti, C.; Beliavski, M.; Tarre, S.; Avrahami, R.; Zussman, E.; Green, M. Durable Electrospun Microtubes for Encapsulation of Bacteria in Atrazine Bioremediation. *J. Water Process Eng.* **2017**, *19* (May), 205–211. https://doi.org/10.1016/j.jwpe.2017.08.004.

(9) Letnik, I.; Avrahami, R.; Rokem, J. S.; Greiner, A.; Zussman, E.; Greenblatt, C. Living Composites of Electrospun Yeast Cells for Bioremediation and Ethanol Production. *Biomacromolecules* **2015**, *16* (10), 3322–3328. https://doi.org/10.1021/acs.biomac.5b00970.

(10) Dima, P.; Stubbe, P. R.; Mendes, A. C.; Chronakis, I. S. Electric Field Charge Polarity Triggers the Organization and Promotes the Stability of Electrosprayed Probiotic Cells. *Food Hydrocoll.* **2023**, *139* (February), 108549. https://doi.org/10.1016/j.foodhyd.2023.108549.

(11) Mukiri, C.; Raja, K.; Senthilkumar, M.; Subramanian, K. S.; Govindaraju, K.; Pradeep, D.; Ranjan, S. Immobilization of Beneficial Microbe Methylobacterium Aminovorans in Electrospun Nanofibre as Potential Seed Coatings for Improving Germination and Growth of Groundnut Arachis Hypogaea. *Plant Growth Regul.* **2022**, *97* (2), 419–427. https://doi.org/10.1007/s10725-021-00737-1.

(12) De Gregorio, P. R.; Michavila, G.; Muller, L. R.; De Souza Borges, C.; Pomares, M. F.; De Sá, E. L. S.; Pereira, C.; Vincent, P. A. Beneficial Rhizobacteria Immobilized in Nanofibers for Potential Application as Soybean Seed Bioinoculants. *PLoS One* **2017**, *12* (5), 1–22. https://doi.org/10.1371/journal.pone.0176930.

(13) Hussain, Z.; Khan, M. A.; Iqbal, F.; Raffi, M.; Hafeez, F. Y. Electrospun Microbial-Encapsulated Composite-Based Plasticized Seed Coat for Rhizosphere Stabilization and Sustainable Production of Canola (Brassica Napus L.). *J. Agric. Food Chem.* **2019**, *67* (18), 5085–5095. https://doi.org/10.1021/acs.jafc.8b06505.

(14) Shin, Y.; Lee, J.; Kim, M.; Park, J.; Kim, S.; Kim, J.; Oh, J.-W.; Han, D.-W. Biomimetic Hybrid Nanofiber Sheets Composed of RGD Peptide-Decorated PLGA as Cell-Adhesive Substrates. *J. Funct. Biomater.* **2015**, *6* (2), 367–378. https://doi.org/10.3390/jfb6020367.

(15) Wu, L.; Zang, J.; Lee, L. A.; Niu, Z.; Horvatha, G. C.; Braxtona, V.; Wibowo, A. C.; Bruckman, M. A.; Ghoshroy, S.; Zur Loye, H. C.; Li, X.; Wang, Q. Electrospinning Fabrication, Structural and Mechanical Characterization of Rod-like Virus-Based Composite Nanofibers. *J. Mater. Chem.* **2011**, *21* (24), 8550–8557. https://doi.org/10.1039/c1jm00078k.

(16) Zhang, C.; Li, Y.; Wang, P.; Zhang, H. Electrospinning of Nanofibers: Potentials and Perspectives for Active Food Packaging. *Compr. Rev. Food Sci. Food Saf.* **2020**, *19* (2), 479–502. https://doi.org/10.1111/1541-4337.12536.

(17) Rosner, D.; Clark, J. Formulations for Bacteriophage Therapy and the Potential Uses of Immobilization. *Pharmaceuticals* **2021**, *14* (4). https://doi.org/10.3390/ph14040359.

(18) Tang, C.; Ozcam, A. E.; Stout, B.; Khan, S. A. Effect of PH on Protein Distribution in Electrospun PVA/BSA Composite Nanofibers. *Biomacromolecules* **2012**, *13* (5), 1269–1278. https://doi.org/10.1021/bm2017146.

(19) Bonino, C. A.; Efimenko, K.; Jeong, S. I.; Krebs, M. D.; Alsberg, E.; Khan, S. A. Three-Dimensional Electrospun Alginate Nanofiber Mats via Tailored Charge Repulsions. *Small* **2012**, *8* (12), 1928–1936. https://doi.org/10.1002/smll.201101791.

(20) Mu, X.; Liu, Y.; Fang, D.; Wang, Z.; Nie, J.; Ma, G. Electric Field Induced Phase Separation on Electrospinning Polyelectrolyte Based Core – Shell Nanofibers. *Carbohydr. Polym.* **2012**, *90* (4), 1582–1586. https://doi.org/10.1016/j.carbpol.2012.07.034.

(21) Urbanek, O.; Sajkiewicz, P.; Pierini, F. The Effect of Polarity in the Electrospinning Process on PCL / Chitosan Nano Fi Bres ' Structure , Properties and Ef Fi Ciency of Surface Modi Fi Cation. **2017**, *124*, 168–175. https://doi.org/10.1016/j.polymer.2017.07.064.

(22) Li, Z.; Kang, H.; Che, N.; Liu, Z.; Li, P.; Li, W.; Zhang, C.; Cao, C.; Liu, R.; Huang, Y. Effects of Electrode Reversal on the Distribution of Naproxen in the Electrospun Cellulose Acetate Nanofibers. *J. Nanomater.* **2014**, *2014*. https://doi.org/10.1155/2014/360658.

(23) Lee, S. W.; Belcher, A. M. Virus-Based Fabrication of Micro- and Nanofibers Using Electrospinning. *Nano Lett.* **2004**, *4* (3), 387–390. https://doi.org/10.1021/nl034911t.

(24) Shin, Y. C.; Lee, J. H.; Jin, L.; Kim, M. J.; Oh, J. W.; Kim, T. W.; Han, D. W. Cell-Adhesive RGD Peptide-Displaying M13 Bacteriophage/PLGA Nanofiber Matrices for Growth of Fibroblasts. *Biomater. Res.* **2014**, *18* (1), 1–7. https://doi.org/10.1186/2055-7124-18-14.

(25) Safari, Z.; Soudi, S.; Jafarzadeh, N.; Hosseini, A. Z.; Vojoudi, E.; Sadeghizadeh, M.

Promotion of Angiogenesis by M13 Phage and RGD Peptide in Vitro and in Vivo. *Sci. Rep.* **2019**, *9* (1), 11182. https://doi.org/10.1038/s41598-019-47413-z.

(26) Sugimoto, R.; Lee, J. H.; Lee, J. H.; Jin, H. E.; Yoo, S. Y.; Lee, S. W. Bacteriophage Nanofiber Fabrication Using near Field Electrospinning. *RSC Adv.* **2019**, *9* (67), 39111–39118. https://doi.org/10.1039/c9ra07510k.

(27) Branston, S. D.; Stanley, E. C.; Ward, J. M.; Keshavarz-Moore, E. Determination of the Survival of Bacteriophage M13 from Chemical and Physical Challenges to Assist in Its Sustainable Bioprocessing. *Biotechnol. Bioprocess Eng.* **2013**, *18* (3), 560–566. https://doi.org/10.1007/s12257-012-0776-9.

(28) Huang, Y.; Chiang, C. Y.; Lee, S. K.; Gao, Y.; Hu, E. L.; De Yoreo, J.; Belcher, A. M. Programmable Assembly of Nanoarchitectures Using Genetically Engineered Viruses. *Nano Lett.* **2005**, *5* (7), 1429–1434. https://doi.org/10.1021/nl050795d.

(29) Zaman, M. S.; Moon, C. H.; Bozhilov, K. N.; Haberer, E. D. Phage-Directed Synthesis of Copper Sulfide: Structural and Optical Characterization. *Nanotechnology* **2013**, *24* (32). https://doi.org/10.1088/0957-4484/24/32/325602.

(30) Petrenko, V. A.; Smith, G. P. Phages from Landscape Libraries as Substitute Antibodies. *Protein Eng.* **2000**, *13* (8), 589–592. https://doi.org/10.1093/protein/13.8.589.

(31) Passaretti, P.; Sun, Y.; Dafforn, T. R.; Oppenheimer, P. G. Determination and Characterisation of the Surface Charge Properties of the Bacteriophage M13 to Assist Bio-Nanoengineering. *RSC Adv.* **2020**, *10* (42), 25385–25392. https://doi.org/10.1039/d0ra04086j.

(32) Cheeney, J. E.; Hsieh, S. T.; Myung, N. V.; Haberer, E. D. Whispering Gallery Mode Emission from Dye-Doped Polymer Fiber Cross-Sections Fabricated by near-Field Electrospinning. *Nanoscale* **2020**, *12* (17), 9873–9883. https://doi.org/10.1039/d0nr00147c.

(33) Lam, C. C.; Leung, P. T.; Young, K. Explicit Asymptotic Formulas for the Positions, Widths, and Strengths of Resonances in Mie Scattering. *J. Opt. Soc. Am. B* **1992**, *9* (9), 1585. https://doi.org/10.1364/josab.9.001585.

(34) Khozeymeh, F.; Razaghi, M. Cylindrical Optical Resonators: Fundamental Properties and Bio-Sensing Characteristics. *J. Opt. (United Kingdom)* **2018**, *20* (4), 45301. https://doi.org/10.1088/2040-8986/aab052.

(35) Arnold, S.; Khoshsima, M.; Teraoka, I.; Holler, S.; Vollmer, F. Shift of Whispering-Gallery Modes in Microspheres by Protein Adsorption. *Opt. Lett.* **2003**, *28* (4), 272. https://doi.org/10.1364/ol.28.000272.

(36) Landry, J. P.; Sun, Y. S.; Guo, X. W.; Zhu, X. D. Protein Reactions with Surface-Bound Molecular Targets Detected by Oblique-Incidence Reflectivity Difference Microscopes. *Appl. Opt.* **2008**, *47* (18), 3275–3288. https://doi.org/10.1364/AO.47.003275.

(37) Li, T.; Zan, X.; Sun, Y.; Zuo, X.; Li, X.; Senesi, A.; Winans, R. E.; Wang, Q.; Lee, B. Self-Assembly of Rodlike Virus to Superlattices. *Langmuir* **2013**, *29* (41), 12777–12784. https://doi.org/10.1021/la402933q.

(38) Collins, G.; Federici, J.; Imura, Y.; Catalani, L. H. Charge Generation, Charge Transport, and Residual Charge in the Electrospinning of Polymers: A Review of Issues and Complications. *J. Appl. Phys.* **2012**, *111* (4), 1–18. https://doi.org/10.1063/1.3682464.

(39) Li, Z.; Liu, R.; Huang, Y.; Zhou, J. Effects of Reversed Arrangement of Electrodes on Electrospun Nanofibers. *J. Appl. Polym. Sci.* **2017**, *134* (15), 1–8. https://doi.org/10.1002/app.44687.

(40) Gong, C.; Yang, X.; Tang, S. J.; Zhang, Q. Q.; Wang, Y.; Liu, Y. L.; Chen, Y. C.; Peng, G. D.; Fan, X.; Xiao, Y. F.; Rao, Y. J.; Gong, Y. Submonolayer Biolasers for Ultrasensitive Biomarker Detection. *Light Sci. Appl.* **2023**, *12* (1). https://doi.org/10.1038/s41377-023-01335-8.

(41) Ruan, J.; Guo, D.; Niu, B.; Ge, K.; Zhai, T. Whispering-Gallery-Mode Full-Color Laser Textiles and Their Anticounterfeiting Applications. *NPG Asia Mater.* **2022**, *14* (1), 1–7. https://doi.org/10.1038/s41427-022-00408-1.

(42) Toropov, N.; Cabello, G.; Serrano, M. P.; Gutha, R. R.; Rafti, M.; Vollmer, F. Review of Biosensing with Whispering-Gallery Mode Lasers. *Light Sci. Appl.* **2021**, *10* (1). https://doi.org/10.1038/s41377-021-00471-3.

(43) Jiang, X.; Qavi, A. J.; Huang, S. H.; Yang, L. Whispering-Gallery Sensors. *Matter* **2020**, *3* (2), 371–392. https://doi.org/10.1016/j.matt.2020.07.008.

(44) Eversole, J. D.; Lin, H. B.; Merritt, C. D.; Campillo, A. J. Absorption Spectroscopy Using Microdroplet Resonance Fluorescence Intensities. *Appl. Spectrosc.* **1994**, *48* (3), 373–381. https://doi.org/10.1366/0003702944028254.

(45) Jiang, X.; Qavi, A. J.; Huang, S. H.; Yang, L. Review Whispering-Gallery Sensors. *Matter* **2020**, *3* (2), 371–392. https://doi.org/10.1016/j.matt.2020.07.008.

(46) Vollmer, F.; Arnold, S. Whispering-Gallery-Mode Biosensing: Label-Free Detection down

to Single Molecules. *Nat. Methods* **2008**, *5* (7), 591–596. https://doi.org/10.1038/nmeth.1221.

(47) Zhu, H.; White, I. M.; Suter, J. D.; Zourob, M.; Fan, X. Opto-Fluidic Micro-Ring Resonator for Sensitive Label-Free Viral Detection. *Analyst* **2008**, *133* (3), 356–360. https://doi.org/10.1039/b716834a.

(48) Vafapour, Z.; Ghahraloud, H.; Keshavarz, A.; Islam, M. S.; Rashidi, A.; Dutta, M.; Stroscio, M. A. The Potential of Refractive Index Nanobiosensing Using a Multi-Band Optically Tuned Perfect Light Metamaterial Absorber. *IEEE Sens. J.* **2021**, *21* (12), 13786–13793. https://doi.org/10.1109/JSEN.2021.3070731.